Uplink Interference Analysis With RF Switching for Lens–Based Millimeter–Wave Systems

Uplink Interference Analysis With RF Switching for Lens–Based Millimeter–Wave Systems

Harsh Tataria*, Michail Matthaiou*, Peter J. Smith†, George C. Alexandropoulos‡, and Vincent F. Fusco*
*Institute of Electronics, Communications and Information Technology (ECIT), Queen's University Belfast, Belfast, U.K.
†School of Mathematics and Statistics, Victoria University of Wellington, Wellington, New Zealand
‡Mathematical and Algorithmic Sciences Lab, Paris Research Center, Huawei Technologies France SASU, France
e–mail:{h.tataria, m.matthaiou, v.fusco}@qub.ac.uk, peter.smith@vuw.ac.nz, george.alexandropoulos@huawei.com

***Abstract*—In this paper, we take a fundamental look at the interference characteristics of a lens–based millimeter–wave multiuser multiple–input multiple–output system. We consider a hybrid architecture, implemented via a bank of radio–frequency (RF) switches which perform beam selection followed by low–complexity uplink maximum–ratio combining at baseband. Considering a Rotman lens antenna array in line–of–sight propagation, we derive tight analytical expressions for the average (expected) interference power of an arbitrary user terminal, with and without the presence of RF switching. Our mathematical expressions show that without RF switching, the Rotman lens losses its benefits and collapses to a conventional uniform linear array. Numerical results demonstrate that the expected interference power of a given terminal decreases significantly with RF switching, due to the beam selection process separating multiple uplink direction–of–arrivals (DoAs). This is in contrast to the case when there is no RF switching, which relaxes the beam selection constraints and thus allows very similar DoAs. Overall, the results in this paper emphasize the necessity of RF switching in order to obtain superior performance with a Rotman lens array, over conventional phased arrays.**

I. Introduction

With large transmission bandwidths on offer, cellular communication over millimeter–wave (mmWave) frequencies has emerged as a key concept for future mobile broadband access [1]. However, operation of cellular systems at such high frequencies has also led to new engineering challenges, which need to be overcome before adoption on a scale commensurate with their true potential. In stark contrast to conventional systems which operate below 6 GHz, electromagnetic propagation at mmWave is substantially different (see e.g., [1–3]). Firstly, large array gains are required in order to overcome the high propagation losses at mmWave frequencies. Consequently, either massive antenna arrays or highly directive elements are needed to facilitate transmission over moderately large distances. Secondly, mmWaves do not penetrate solid objects well. As a result, the propagation channel is dominated by the presence of unobstructed direct paths, as well as specular reflections. This implies that mmWave links are likely to be sparse and exhibit strong line–of–sight (LoS) components [4].

While placing large numbers of antenna elements in smaller form factors is becoming plausible at mmWave, thanks to the minuscule wavelengths, if conventional multiuser multiple–input multiple–output (MU–MIMO) techniques are employed, the corresponding signal processing complexity and radio frequency (RF) transceiver power consumption is likely to increase dramatically [5, 6]. For both single–user and MU–MIMO systems, extensive efforts have been made to address these issues with cost–effective techniques, such as hybrid analog–digital (RF–baseband) processing (see e.g., [5–11]). The premise of hybrid processing is to reduce the signal dimension in the RF domain with a network of phase shifters or switches, allowing for a reduced number of RF transceivers and lower–dimensional baseband processing. A contemporary summary of [5, 7–11], along with a taxonomy of the various signal processing algorithms proposed in the hybrid architecture literature can be found in [5] and the references therein.

An alternative stream of work on hybrid transceivers utilizes more advanced antenna array designs, such as RF lenses [12–18, 21]. Fundamentally, RF lenses are phase shifting devices, which convert a divergent wavefront from a point source into a plane wave. A common topology reported in the literature is known as a Rotman lens array, which uses a uniform linear array (ULA) of antennas for signal transmission and/or reception [12–14, 18, 21]. In this light, discrete lens arrays (DLAs) were considered for point–to–point MIMO systems in [12, 13]. The DLA concept was based on beamspace MIMO, where uplink/downlink signals sampled on the ULA are equivalently represented in the beamspace domain via a discrete Fourier transformation (DFT) [19]. As shown in [12, 13], for LoS mmWave channels, the equivalent beamspace representation leverages the sparse nature of the propagation channel, and devises a capacity achieving technique called continuous aperture phased MIMO (CAP–MIMO). CAP–MIMO was extended to multiuser mmWave systems in [20]. In addition to the above, the literature also reports a parallel direction of work employing flat RF lenses, where unlike the Rotman structure, the array elements are non–uniformly located on the focal arc of the lens (see for e.g., [15, 16]). The equivalent capacity achieving technique for flat lens arrays is known as path–division multiplexing for both point–to–point and MU–MIMO systems, as demonstrated in [15, 16].

Despite the above efforts in lens–based mmWave systems, it remains an open problem to analytically quantify the amount of performance gain a lens array induces into a MU–MIMO system, in comparison to conventional phased arrays. To the best of the authors' knowledge, there has been no study which makes such a direct comparison. Characterizing this difference is critical in order to gain a fundamental understanding of the operational differences between lens arrays and conventional phased arrays at mmWave frequencies. In this paper, we bridge

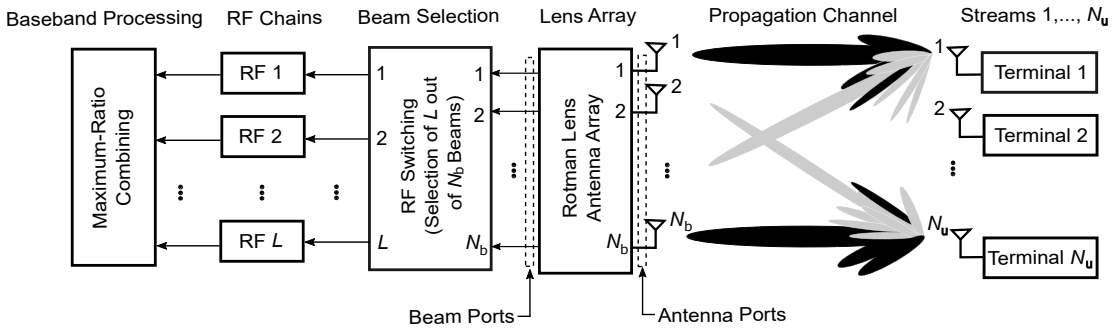

Fig. 1. Hybrid (RF–baseband) uplink MU–MIMO system model with a Rotman lens embedded receive antenna array.

the aforementioned gap. In particular, considering a Rotman lens array at a cellular BS, communicating with multiple single–antenna user terminals, we derive tight analytical expressions for the expected uplink interference power at an arbitrary terminal under LoS propagation; as it is envisaged to be a dominant feature in mmWave channels. In doing this, we assume both full baseband processing (i.e., no RF switching) with maximum–ratio combining (MRC), as well as hybrid processing with RF switching to perform beam selection, followed by low–complexity MRC. Our analysis shows that without RF switching, the Rotman lens simplifies to a conventional ULA, and all its benefits vanish. The numerical results demonstrate that the expected interference power is significantly lower with RF switching, due to the separation of multiple random DoAs during the beam selection process. This is in contrast to when there is no RF switching, which also caters for very similar DoAs, leading to higher average interference levels. The derivations are extremely difficult to perform due to the aggregate presence of both RF and baseband processing. Hence, to the best of our knowledge, such an analysis missing from the vast literature on hybrid architectures at mmWave frequencies.

Notation. Boldface upper and lower case symbols are used to denote matrices and vectors. The $X \times X$ identity matrix is denoted as $\mathbf{I}_X$. The transpose and Hermitian transpose operations are denoted by $(\cdot)^{\mathrm{T}}$ and $(\cdot)^{\mathrm{H}}$, respectively. We use $\mathbf{x} \sim \mathcal{CN}\left(0, \sigma^2\right)$ to denote independent and identically distributed (i.i.d.) random entries in the vector having complex Gaussian entries with zero–mean and variance σ^2. Furthermore, $x \sim \mathcal{U}\left[a, b\right]$ is used to denote a uniform random variable, x, taking on values from a to b. The statistical expectation is denoted by $\mathbb{E}\left\{\cdot\right\}$, while the scalar norm is denoted by $|\cdot|$. The signum function is denoted as $\mathrm{sgn}\left(\cdot\right)$, while the zeroth order Bessel function of the first kind is denoted by $J_0\left(\cdot\right)$ and the scaled incomplete Bessel function is denoted by $\tilde{J}\left(\cdot,\cdot\right)$. Finally, a random variable x conditioned on y is denoted by $x|y$.

II. System Model and Rotman Lens Architecture

We consider the uplink of a single–cellular system, where the BS array is equipped with a Rotman lens antenna array containing N_{b} elements. MU–MIMO operation is assumed, where the Rotman array receives uplink data streams from N_{u} $(N_{\mathrm{b}} \gg N_{\mathrm{u}})$ single–antenna user terminals, within the same time–frequency resource. The terminals are uniformly distributed with respect to a circular coverage area with radius R. The BS is located at the origin of this circle. Each terminal transmits an independent data stream to the lens array with equal power over a LoS channel. With LoS, the acquisition of a complete channel response is not required, as only the DoAs need to be estimated. With lens arrays, these are possible to recover with sufficient accuracy due to the unique spatial focusing from each antenna port to each beam port. Furthermore, in general, the DoAs vary approximately $40\times$ less frequently than the small–scale parameters and can be acquired over multiple channel coherence intervals via exploitation of channel reciprocity [22]. The Rotman array at the BS decouples the multiplexed data streams with RF and baseband processing. Specifically, RF switching is considered to select $L\left(N_{\mathrm{u}} \leq L \leq N_{\mathrm{b}}\right)$ strongest uplink beams out of N_{b}, significantly reducing the number of RF chains. The resulting dimension–reduced signal is down–converted and digitized for further baseband processing. We employ low–complexity MRC to perform baseband processing at the Rotman array. The overall system architecture is depicted in Fig. 1.

A. Mathematical Modeling of the Rotman Lens Array

The Rotman lens itself is a true time delay beamforming network, which artificially introduces time delays to focus the electromagnetic energy transmitted or received by the antenna array [14]. Figure 2 shows a schematic representation of a Rotman lens with N_{bp} beam ports and N_{ap} antenna ports. Without loss of generality, in this paper, we assume that $N_{\mathrm{bp}} = N_{\mathrm{ap}} = N_{\mathrm{b}}$. The j–th transmission path from antenna ports i and j to the beamport m has the distances $r_{m,i} = d_{m,i} + w_i$ and $r_{m,j} = d_{m,j} + w_j$. Here, w_i is the transmission line length from the i–th antenna port to the i–th linear taper in the array port contour. Furthermore, $d_{m,i}$ is the transmission distance from the i–th linear taper to the m–th beam port. Assuming an inter–element spacing of Δ_{i}, the wave distance $b_{j,i}$ for terminal 1 can be calculated as $b_{j,i} = (j-i)\,\Delta_{\mathrm{i}} \sin\left(\theta_1\right)$. To ensure that a planewave with the DoA θ_1 can be focused at the m–th beamport, the transmission distance between the i–th and j–th paths should compensate the phase differences introduced by $b_{j,i}$, such that the signals can be superimposed constructively. Hence, the beam port and array port contours, as well as the transmission line should be designed aiming to satisfy $k_s\left(r_{m,i} - r_{m,j}\right) = k_0 b_{j,i}$, where k_s and k_0 are the wavenumbers of the lens substrate dielectric material and the air, respectively. The location of beam port

$$\mathbf{S}_{\text{RF}} = \begin{bmatrix} 0 & 0 & 1 & 0 & 0 & 0 & 0 & 0 & 0 & 0 & 0 & 0 & 0 & 0 & 0 & 0 \\ 0 & 0 & 0 & 0 & 0 & 0 & 0 & 1 & 0 & 0 & 0 & 0 & 0 & 0 & 0 & 0 \\ 0 & 0 & 0 & 0 & 0 & 0 & 0 & 0 & 0 & 0 & 1 & 0 & 0 & 0 & 0 & 0 \end{bmatrix}. \tag{1}$$

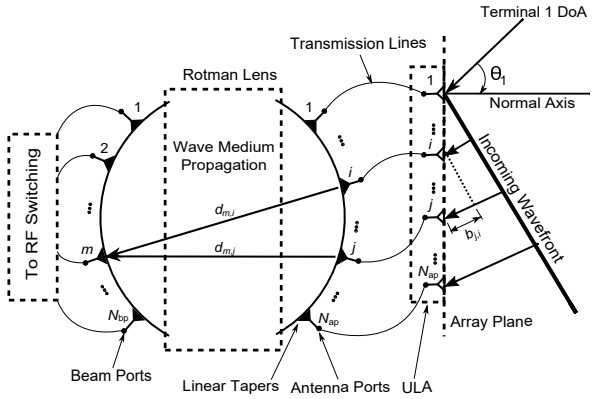

Fig. 2. A Rotman lens antenna array with $N_{\text{ap}} = N_{\text{bp}} = N_{\text{b}}$.

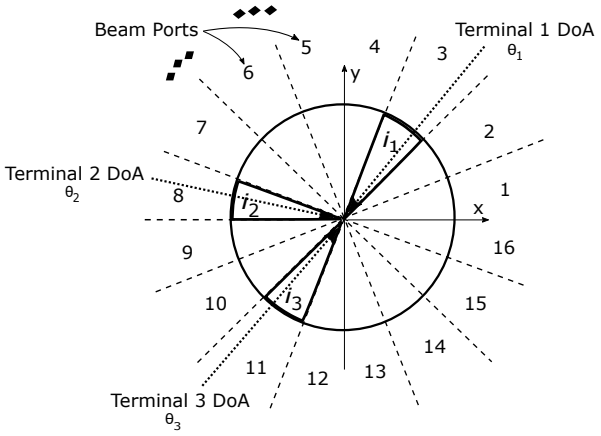

Fig. 3. An example of the RF switch matrix functionality where $N_b = 16$ and $L = 3$. The terminal DoAs randomly excite the available beam ports.

m on the port contour is called the focal point, while the beam port contour is called the focal arc. However, it has been shown in [21] that it is impossible to satisfy this for all of the beam port locations at the same time. Hence, the more practical way to design a Rotman lens is to usually pick at least three focal point locations on the beam port contour, where the contour guarantees limited phase errors to the remaining ports [21]. Considering this, the net effect of the Rotman lens can be described with an $N_{\text{b}} \times N_{\text{b}}$ matrix, $\mathbf{F}_{\text{RM}}$, which captures the incident RF paths from N_{b} antenna elements to form N_{b} spatial beams. In particular, the (m, n)–th entry of $\mathbf{F}_{\text{RM}}$ denotes the scattering parameter from antenna port n to beam port m. For an ideal Rotman lens without any phase errors and insertion losses, $\mathbf{F}_{\text{RM}} = \left[\mathbf{a}(\theta_1), \ldots, \mathbf{a}(\theta_{N_{\text{b}}})\right]^{\text{H}}$, where $\mathbf{a}(\theta_1) = \frac{1}{\sqrt{N_{\text{b}}}}[1, e^{j\frac{2\pi}{\lambda}\Delta_i \sin(\theta_1)}, \ldots, e^{j(N_{\text{b}}-1)\frac{2\pi}{\lambda}\Delta_i \sin(\theta_1)}]^{\text{T}}$, without loss of generality. Here λ is the wavelength corresponding to the carrier frequency. Note that $\theta_1, \ldots, \theta_{N_{\text{b}}}$ are the set of sweeping angles corresponding to the lens beam ports. From a signal processing viewpoint, $\mathbf{F}_{\text{RM}}$ samples the RF signals in the angular domain with fixed angular bins. With LoS propagation, the electromagnetic energy lies in one arbitrary angular bin, which we select with the bank of RF switches. Mathematically, the RF switching functionality can be described with a binary beam selection matrix, $\mathbf{S}_{\text{RF}}$, which selects L rows of $\mathbf{F}_{\text{RM}}$. Hence, $\mathbf{S}_{\text{RF}}$ is an $L \times N_{\text{b}}$ matrix, and each row of it contains only one non–zero value corresponding to the selected beam index. For example, suppose the Rotman lens has $N_{\text{ap}} = N_{\text{bp}} = N_{\text{b}} = 16$. If the third, eight, and eleventh beam ports are going to be selected, then $\mathbf{S}_{\text{RF}}$ would have the structure in (1), given on top of the page. We denote the $L = 3$ selected subports as i_1, i_2, and i_3. We make the assumption that the RF switch matrix selects the L subports with a non–overlapping DoA support set. The switch matrix functionality is shown in Fig. 3, where the DoAs fall within separate bins, where the width of each bin is $2\pi/N_{\text{b}}$.

B. Signal and Propagation Models

Considering the above model of the Rotman lens array, the $L \times 1$ received signal after beam selection is given by

$$\mathbf{y} = \rho_{\text{x}}^{\frac{1}{2}} \mathbf{S}_{\text{RF}} \mathbf{F}_{\text{RM}} \mathbf{H} \mathbf{x} + \mathbf{n}. \tag{2}$$

Here, ρ_{x} is the average transmit power over N_{u} terminals, $\mathbf{H} = [\mathbf{h}_1, \ldots, \mathbf{h}_{N_{\text{u}}}]$ is the $N_b \times N_u$ propagation channel matrix, where $\mathbf{h}_k$ denotes the $N_b \times 1$ vector from terminal k to the Rotman array, and $\mathbf{x}$ is a $N_{\text{u}} \times 1$ vector containing payload data symbols from each terminal to the Rotman array. We note that $\mathbb{E}\left\{\mathbf{x}\mathbf{x}^{\text{H}}\right\} = \frac{1}{N_u}\mathbf{I}_{N_{\text{u}}}$. Furthermore, the $L \times 1$ vector of i.i.d. complex Gaussian noise is denote by $\mathbf{n}$, such that $\mathbf{n} \sim \mathcal{CN}(0, 1)$. Without loss of generality, we consider terminal 1 as the desired terminal of interest. With LoS propagation,

$$\mathbf{h}_1 = \beta_1^{\frac{1}{2}} \mathbf{a}(\theta_1), \tag{3}$$

where $\beta_1 = d_1^{-\gamma}$ is the link gain, composed of distance–dependent geometric attenuation, with d_1 denoting the distance from the Rotman array to terminal 1 and γ denoting the attenuation exponent. The complex array steering vector, $\mathbf{a}(\theta_1)$, follows the structure described earlier. The de–multiplexed signal from terminal 1 after MRC baseband processing can then be written as

$$\begin{aligned} r_1^{\text{RL}} &= (\mathbf{S}_{\text{RF}} \mathbf{F}_{\text{RM}} \mathbf{h}_1)^{\text{H}} \mathbf{y} \\ &= \rho_{\text{x}}^{\frac{1}{2}} \mathbf{h}_1^{\text{H}} (\mathbf{S}_{\text{RF}} \mathbf{F}_{\text{RM}})^{\text{H}} \mathbf{S}_{\text{RF}} \mathbf{F}_{\text{RM}} \mathbf{h}_1 x_1 + \rho_{\text{x}}^{\frac{1}{2}} \sum_{j=2}^{L} \mathbf{h}_1^{\text{H}} (\mathbf{S}_{\text{RF}} \mathbf{F}_{\text{RM}})^{\text{H}} \\ &\quad \times \mathbf{S}_{\text{RF}} \mathbf{F}_{\text{RM}} \mathbf{h}_j x_j + \mathbf{h}_1^{\text{H}} (\mathbf{S}_{\text{RF}} \mathbf{F}_{\text{RM}})^{\text{H}} \mathbf{n}, \end{aligned} \tag{4}$$

where the first term denotes the desired signal, second term denotes the multiuser interference, and the third term is the additive Gaussian noise across the selected and processed beams. The corresponding SINR for terminal 1 can then be written as in (5) on top of the following page.

Remark 1. A closer look at (5) tells us that with MRC processing in LoS, the desired signal and noise powers are only a function of θ_1, and are therefore deterministic quantities. In contrast, the uncertainty lies in the interference power, which depends on the remaining $L-1$ selected beams, making it the most important term for performance characterization. While in the subsequent section we compute the average interfer-

$$\mathrm{SINR}_1^{\mathrm{RL}} = \frac{\rho_{\mathrm{x}} \left| \mathbf{h}_1^{\mathrm{H}} \left(\mathbf{S}_{\mathrm{RF}} \mathbf{F}_{\mathrm{RM}} \right)^{\mathrm{H}} \mathbf{S}_{\mathrm{RF}} \mathbf{F}_{\mathrm{RM}} \mathbf{h}_1 x_1 \right|^2}{\left| \mathbf{h}_1^{\mathrm{H}} \left(\mathbf{S}_{\mathrm{RF}} \mathbf{F}_{\mathrm{RM}} \right)^{\mathrm{H}} \mathbf{n} \right|^2 + \rho_{\mathrm{x}} \sum_{j=2}^{L} \left| \mathbf{h}_1^{\mathrm{H}} \left(\mathbf{S}_{\mathrm{RF}} \mathbf{F}_{\mathrm{RM}} \right)^{\mathrm{H}} \mathbf{S}_{\mathrm{RF}} \mathbf{F}_{\mathrm{RM}} \mathbf{h}_j x_j \right|^2}. \tag{5}$$

ence power, we note that in the absence of RF switching, $\mathbf{S}_{\mathrm{RF}} = \mathbf{I}_{N_{\mathrm{b}}}$, and $\mathbf{F}_{\mathrm{RM}}^{\mathrm{H}} \mathbf{F}_{\mathrm{RM}} = \mathbf{I}_{N_{\mathrm{b}}}$, due to $\mathbf{F}_{\mathrm{RM}}$ being a unitary DFT matrix. Under this special scenario, the Rotman lens structure collapses to a conventional ULA and loses the benefits of the RF lens. This demonstrates the necessity of a switch matrix to leverage the full benefit of a Rotman lens. In addition, removal of RF switching implies removal of the beam selection process, and consequently the system losses its ability to perform hybrid processing, converging to full baseband operation with a ULA and N_{b} RF transceivers.

III. Expected Interference Power Analysis With RF Switching

A. Integrals and Special Functions

Before presenting the main analytical contributions, we define and evaluate the key integrals and special functions which are used throughout the paper. In particular,

$$\begin{aligned} Q\left(a,b,v,z,\theta\right) &= \int_a^b e^{\,j\frac{2\pi}{\lambda}(v-z)\Delta_{\mathrm{i}}\sin(\theta)}\, d\theta \\ &= \int_a^b e^{\,j\frac{2\pi}{\lambda}(v-z)\Delta_{\mathrm{i}}\cos\left(\theta-\frac{\pi}{2}\right)}\, d\theta. \end{aligned} \tag{6}$$

To evaluate the integral in (6), we let $\kappa = j\frac{2\pi}{\lambda}\left(v-z\right)\Delta_{\mathrm{i}}$, and substitute θ with x. Furthermore, we denote $J\left(a,b,\kappa,x\right) = \int_{a-\frac{\pi}{2}}^{b-\frac{\pi}{2}} e^{\kappa\cos(x)}dx$, and $\tilde{J}\left(0,\theta,\kappa,x\right) = \int_0^{\theta} e^{\kappa\cos(x)}dx$. We recognize that $J\left(a,b,\kappa,x\right)$ can be evaluated in terms of $\tilde{J}\left(0,\theta,\kappa,x\right)$, via the three piecewise cases listed below:
1) $a > \frac{\pi}{2}$: $J\left(a,b,\kappa,x\right) = \tilde{J}\left(0,b-\frac{\pi}{2},\kappa,x\right) - \tilde{J}\left(0,a-\frac{\pi}{2},\kappa,x\right)$.
2) $b > \frac{\pi}{2}$ and $a < \frac{\pi}{2}$: $J\left(a,b,\kappa,x\right) = \tilde{J}\left(0,b-\frac{\pi}{2},\kappa,x\right) + \int_{a-\frac{\pi}{2}}^{0} e^{\kappa\cos(x)}dx = \tilde{J}\left(0,b-\frac{\pi}{2},\kappa,x\right) + \tilde{J}\left(0,a-\frac{\pi}{2},\kappa,x\right)$, by exploiting symmetry in the integrals.
3) $a < \frac{\pi}{2}$: $J\left(a,b,\kappa,x\right) = -\tilde{J}\left(0,b-\frac{\pi}{2},\kappa,x\right) + \tilde{J}\left(0,a-\frac{\pi}{2},\kappa,x\right)$.
Then, we have $J\left(a,b,\kappa,x\right) = \mathrm{sgn}\left(b-\frac{\pi}{2}\right)\tilde{J}\left(0,b-\frac{\pi}{2},\kappa,x\right) - \mathrm{sgn}\left(a-\frac{\pi}{2}\right)\tilde{J}\left(0,a-\frac{\pi}{2},\kappa,x\right)$. Substituting κ and θ back,

$$\begin{aligned} Q\left(a,b,v,z,\theta\right) =& \int_a^b e^{\,j\frac{2\pi}{\lambda}(v-z)\Delta_{\mathrm{i}}\sin(\theta)}\, d\theta \\ =& \mathrm{sgn}\left(b-\frac{\pi}{2}\right)\tilde{J}\left(0,b-\frac{\pi}{2},j\frac{2\pi}{\lambda}(v-z)\Delta_{\mathrm{i}},\theta\right) \\ &- \mathrm{sgn}\left(a-\frac{\pi}{2}\right)\tilde{J}\left(0,a-\frac{\pi}{2},j\frac{2\pi}{\lambda}(v-z)\Delta_{\mathrm{i}},\theta\right). \end{aligned} \tag{7}$$

As shown in [23], $\tilde{J}\left(\cdot,\cdot,\cdot,\cdot\right)$ is also a scaled incomplete Bessel function, which can be used for efficient numerical evaluation.

B. Analysis Methodology

To simplify the notation, we denote $\mathbf{T} = \mathbf{S}_{\mathrm{RF}}\mathbf{F}_{\mathrm{RM}}$. Then from (5), the instantaneous interference power averaged over the interfering payload data symbols can be written as $I_1^{\mathrm{RL}} = \rho_{\mathrm{x}}\sum_{j=2}^{L}\left|\mathbf{h}_1^{\mathrm{H}}\mathbf{T}^{\mathrm{H}}\mathbf{T}\,\mathbf{h}_j\right|^2 \mathrm{E}_{\mathrm{x}}$, where $\mathrm{E}_{\mathrm{x}} = \mathbb{E}\left\{|x_j|^2\right\} = 1, \forall j = 2,\ldots,L$. The expected value of I_1^{RL}, averaged over the selected directions, can be written as

$$I_1^{\mathrm{RL}} = \rho_{\mathrm{x}}\left(L-1\right)\mathbb{E}\left\{\left|\mathbf{h}_1^{\mathrm{H}}\,\mathbf{T}^{\mathrm{H}}\,\mathbf{T}\,\mathbf{h}_j\right|^2\right\}. \tag{8}$$

Remark 2. In the analysis which follows, we evaluate the expected value in (8). At first sight, analyzing the expectation in (8) may seem straightforward. However, this is not the case, as with RF switching, both $\mathbf{h}_1$ and $\mathbf{h}_j$ could lie in distinct bins (see Fig. 3 for an example), and the remaining $L-2$ bins which define $\mathbf{T}$ could be any given set of bins from a total of $N_{\mathrm{b}}-2$ bins. Therefore, since the bins matter, the nature of the problem becomes combinatorial. Without any simplifications, this would require analyzing $N_{\mathrm{b}}!/\left(L!\left(N_{\mathrm{b}}-L\right)!\right)$ combinations. Naturally, this is problematic for massive lens arrays. Despite this, in our calculations, we overcome these difficulties and propose a general analysis methodology method to compute the required expectation.

Likewise, the DoA of terminal 1 could fall within any of the N_{b} bins. Suppose that the bins are selected with probabilities $p_1,\ldots,p_{N_{\mathrm{b}}}$. Then, we denote an arbitrary beam with a given DoA falling in the k–th bin by $\mathbf{h}_k$. This allows us to write

$$I_1^{\mathrm{RL}} = \rho_{\mathrm{x}}\left(L-1\right)\sum_{k=1}^{N_{\mathrm{b}}} p_k \sum_{\substack{r=1\\ r\neq k}}^{N_{\mathrm{b}}} p_{r|k}\,\mathbb{E}\left\{\left|\mathbf{h}_k^{\mathrm{H}}\mathbf{T}^{\mathrm{H}}\mathbf{T}\,\mathbf{h}_r\right|^2\right\}, \tag{9}$$

where $p_{k|r}$ is the probability that an arbitrary terminal's DoA falls in bin r, given that bin k is occupied. Via straightforward conditional probability theory, we know that $p_{r|k} = p_r/\left(1-p_k\right)$, allowing us to further express I_1^{RL} as

$$I_1^{\mathrm{RL}} = \rho_{\mathrm{x}}\left(L-1\right)\sum_{k=1}^{N_{\mathrm{b}}}\sum_{\substack{r=1\\ r\neq k}}^{N_{\mathrm{b}}}\frac{p_k\,p_r}{1-p_k}\,\mu_{k,r}, \tag{10}$$

where $\mu_{k,r} = \mathbb{E}\left\{|\mathbf{h}_k^{\mathrm{H}}\,\mathbf{T}^{\mathrm{H}}\,\mathbf{T}\,\mathbf{h}_r|^2\right\}$, and $\mathbf{T} = [\mathbf{t}_1,\ldots,\mathbf{t}_L]$. Now, $\mu_{k,r}$ can be written as

$$\begin{aligned} \mu_{k,r} &= \mathbb{E}\left\{\left|\sum_{i=1}^{L}\mathbf{h}_k^{\mathrm{H}}\mathbf{t}_i^{\mathrm{H}}\mathbf{t}_i\,\mathbf{h}_r\right|^2\right\} \\ &= \sum_{i=1}^{L}\sum_{q=1}^{L}\mathbb{E}\left\{\mathbf{h}_k^{\mathrm{H}}\mathbf{t}_i^{\mathrm{H}}\mathbf{t}_i\mathbf{h}_r\mathbf{h}_r^{\mathrm{H}}\mathbf{t}_q^{\mathrm{H}}\mathbf{t}_q\mathbf{h}_k\right\}. \end{aligned} \tag{11}$$

In order to evaluate the expectation on the right hand side of (11), one has to note that i and q could take on any arbitrary value, such that $i \neq k$ and r, $q \neq k$ and r, as well as $i \neq q$. This results in nine cases for which the expectation has to be analyzed. We denote $\chi\left(k,r,i,q\right) = \mathbf{h}_k^{\mathrm{H}}\mathbf{t}_i^{\mathrm{H}}\mathbf{t}_i\,\mathbf{h}_r\,\mathbf{h}_r^{\mathrm{H}}\mathbf{t}_q^{\mathrm{H}}\mathbf{t}_q\,\mathbf{h}_k$ and $\delta_{k,r,i,q} = \mathbb{E}\left\{\chi\left(k,r,i,q\right)\right\}$ as the general case. Then, $\mu_{k,r}$ can be written as (12) (shown on top of the following page for space reasons), where C1 to C9 denote the nine cases.

Remark 3. As highlighted in boldface, C3, C5, C6, C8 and C9 involve a conditional probability. Specifically, C3 is weighted by $p_{i,q|k,r}$, C5 and C6 are weighted by $p_{q|k,r}$, while C8 and C9 are weighted by $p_{i|k,r}$. Physically, $p_{i,q|k,r}$ denotes the probability that two arbitrary DoAs fall in bins i and q, given bins k and r are occupied at the same time.

$$\mu_{k,r} = \sum_{i=1}^{L}\sum_{q=1}^{L} \underbrace{\delta_{k,r,k,k}}_{\text{C1}} + \underbrace{\delta_{k,r,r,r}}_{\text{C2}} + \underbrace{\left((L-2)^2 - (L-2)\right)\delta_{k,r,i,q} + (L-2)\,\delta_{k,r,i,q}}_{\textbf{C3}} + \underbrace{\delta_{k,r,k,r}}_{\text{C4}}$$
$$+ \underbrace{(L-2)\,\delta_{k,r,k,q}}_{\textbf{C5}} + \underbrace{(L-2)\,\delta_{k,r,r,q}}_{\textbf{C6}} + \underbrace{\delta_{k,r,r,k}}_{\text{C7}} + \underbrace{(L-2)\,\delta_{k,r,i,k}}_{\textbf{C8}} + \underbrace{(L-2)\,\delta_{k,r,i,r}}_{\textbf{C9}}. \quad (12)$$

Similarly, $p_{q|k,r}$ and $p_{i|k,r}$ are the probabilities that an arbitrary DoA falls either in bin q or bin i given that bins k and r are occupied. Furthermore, the averaging in C3 is over an ensemble where both $i, q \neq k, r$, where the averaging in C5, C6, C8 and C9 is over an ensemble where either $i, q \neq k, r$. The specific conditional probabilities are given by: $p_{i,q|k,r} = (p_i/(1-p_k-p_r)) \times (p_q/(1-p_k-p_r-p_i))$, $p_{q|k,r} = p_q/(1-p_k-p_r)$ and $p_{i|k,r} = p_i/(1-p_k-p_r)$.

Further simplifying (12), one can write

$$\mu_{k,r} = (\delta_{k,r,k,k} + \delta_{k,r,r,r} + \delta_{k,r,k,r} + \delta_{k,r,r,k}) + (L-2) \times \left[\delta_{k,r,i,i} + \delta_{k,r,k,q} + \delta_{k,r,r,q} + \delta_{k,r,i,k} + \delta_{k,r,i,r}\right] + (L-2)(L-3)\left[\delta_{k,r,i,q}\right], \quad (13)$$

with the unknowns in $\delta_{k,r,i,q}$, for $k = 1,\ldots,N_\text{b}$, $r = 1,\ldots,N_\text{b}$, $r \neq k$, $i = 1,\ldots,N_\text{b}$, and $q = 1,\ldots,N_\text{b}$. In order to analyze $\delta_{k,r,i,q}$, we first need to compute $\chi(k,r,i,q)$, with the restriction that $k \neq r$. This is given by

$$\chi(k,r,i,q) = \frac{1}{N_\text{b}^2}\sum_{s=1}^{N_\text{b}}\sum_{t=1}^{N_\text{b}}\sum_{v=1}^{N_\text{b}}\sum_{z=1}^{N_\text{b}} e^{j\frac{2\pi}{\lambda}(t-s)\Delta_\text{i}\sin(\theta_i)} \times e^{j\frac{2\pi}{\lambda}(z-v)\Delta_\text{i}\sin(\theta_q)}\mathbf{h}_{k,s}^*\,\mathbf{h}_{k,z}\,\mathbf{h}_{r,v}^*\mathbf{h}_{r,t}, \quad (14)$$

as $\mathbf{h}_k^\text{H}\,\mathbf{t}_i^\text{H} = \sum_{s=1}^{N_\text{b}}\mathbf{h}_{k,s}^*\frac{1}{\sqrt{N_\text{b}}}e^{-j\frac{2\pi}{\lambda}(s-1)\Delta_\text{i}\sin(\theta_i)}$, and $\mathbf{t}_i\,\mathbf{h}_r = \sum_{t=1}^{N_\text{b}}\frac{1}{\sqrt{N_\text{b}}}e^{j\frac{2\pi}{\lambda}(t-1)\Delta_\text{i}\sin(\theta_i)}\,\mathbf{h}_{r,t}$. Taking the expected value of (14) yields

$$\delta_{k,r,i,q} = \frac{1}{N_\text{b}^2}\sum_{s=1}^{N_\text{b}}\sum_{t=1}^{N_\text{b}}\sum_{v=1}^{N_\text{b}}\sum_{z=1}^{N_\text{b}} e^{j\frac{2\pi}{\lambda}(t-s)\Delta_\text{i}\sin(\theta_i)} \times e^{j\frac{2\pi}{\lambda}(z-v)\Delta_\text{i}\sin(\theta_q)}\,\mathbb{E}\left\{\mathbf{h}_{k,s}^*\,\mathbf{h}_{k,z}\,\mathbf{h}_{r,v}^*\mathbf{h}_{r,t}\right\}. \quad (15)$$

Recognizing that $\mathbf{h}_k$ and $\mathbf{h}_r$ are statistically independent, one only needs to compute $\mathbb{E}\{\mathbf{h}_{k,s}^*\mathbf{h}_{k,z}\} = \alpha_{k,s,z}$, in order to evaluate $\mathbb{E}\{\mathbf{h}_{k,s}^*\mathbf{h}_{k,z}\mathbf{h}_{r,v}^*\mathbf{h}_{r,t}\} = \alpha_{k,s,z}\alpha_{r,v,t}$. Recalling the fact that the propagation channel can be written as a product of the array steering vector having a DoA θ_k, and its associated link gain β_k for $\mathbf{h}_{k,s}$ and $\mathbf{h}_{k,z}$ in bin c,

$$\alpha_{k,s,z} = \beta_k\,\mathbb{E}\left\{e^{-j\frac{2\pi}{\lambda}(s-1)\Delta_\text{i}\sin(\theta_k)}e^{j\frac{2\pi}{\lambda}(z-1)\Delta_\text{i}\sin(\theta_k)}\right\} = \beta_k\,\mathbb{E}\left\{e^{j\frac{2\pi}{\lambda}(z-s)\Delta_\text{i}\sin(\theta_k)}\right\}. \quad (16)$$

Evaluating the expectation in (16) by first principles, we require $\int_0^{2\pi} e^{j\frac{2\pi}{\lambda}\Delta_\text{i}(z-s)\sin(\theta_k)} f(\theta_k)\,d\theta_k$. Now, $f(\theta_k)$ is a truncated (conditional) probability density function of θ_k, as it is conditioned on being in bin c. Note that this is in contrast to the original distribution which spans $[0, 2\pi]$. Hence, the range of the density is modified to $(2c-3)\frac{\pi}{N_\text{b}} \leq \theta_k \leq (2c-1)\frac{\pi}{N_\text{b}}$, $\forall c = 1,\ldots,N_\text{b}$. As a result, $f(\theta_k)$ translates into $f_c(\theta_k) = f(\theta_k)/q_k$, where $q_k = \text{Probability}(\theta_k \text{ lies in bin } c) = \int_{(2c-3)\frac{\pi}{N_\text{b}}}^{(2c-1)\frac{\pi}{N_\text{b}}} f(\theta_k)\,d\theta_k$. Taking the above into account,

$$\alpha_{k,s,z} = \frac{\beta_k\int_{(2c-3)\frac{\pi}{N_\text{b}}}^{(2c-1)\frac{\pi}{N_\text{b}}} e^{j\frac{2\pi}{\lambda}(z-s)\Delta_\text{i}\sin(\theta_k)} f(\theta_k)\,d\theta_k}{\int_{(2c-3)\frac{\pi}{N_\text{b}}}^{(2c-1)\frac{\pi}{N_\text{b}}} f(\theta_k)\,d\theta_k}. \quad (17)$$

Naturally, $\alpha_{k,s,z}$ is a function of the angular distribution of θ_k. In this study, we consider $\theta_k \sim \mathcal{U}[0, 2\pi]$, and thus

$$\alpha_{k,s,z} = \frac{\beta_k}{\left[(2c-1)\frac{\pi}{N_\text{b}}\right] - \left[(2c-3)\frac{\pi}{N_\text{b}}\right]} \quad (18)$$
$$\times\, Q\left((2c-3)\frac{\pi}{N_\text{b}}, (2c-1)\frac{\pi}{N_\text{b}}, z, s, \theta_k\right), \quad (19)$$

where $Q(\cdot,\cdot,\cdot,\cdot,\cdot)$ is evaluated as in (7), and can also be written as a scaled incomplete Bessel function [23]. The result from (18) can be substituted into the relevant term of (13).

Remark 4. We note that $\alpha_{r,v,t}$ can now be computed following the same routine as for $\alpha_{k,s,z}$. Substituting $\alpha_{k,s,z}\alpha_{r,v,t}$ into $\mathbb{E}\{\mathbf{h}_{k,s}^*\mathbf{h}_{k,z}\mathbf{h}_{r,v}^*\mathbf{h}_{r,t}\}$ yields $\delta_{k,r,i,q}$. Following the above method, each term of $\mu_{k,r}$ in (13) can be computed as a function of $Q(\cdot,\cdot,\cdot,\cdot,\cdot)$. Due to space limitations, we avoid duplicating the analysis and writing out each term of $\mu_{k,r}$. Substituting the expression for $\mu_{k,r}$ into (10) yields the desired result, concluding the method. It is noteworthy that since the Rotman lens array utilizes the ULA, the above analysis can also be applied to a conventional ULA with beam selection (i.e., neglecting the presence of $\mathbf{F}_\text{RM}$), with the following subtle difference: Instead of the RF switching selecting terminal DoAs which fall into different angular bins (the case for Rotman lens array), for a ULA, the RF switching would select DoAs to satisfy a minimum angular separation between two DoAs, i.e., $\cos(\theta_k) - \cos(\theta_r)$, for any two DoAs in k and r. This requires no change in the analysis methodology.

IV. Expected Interference Power Analysis Without RF Switching

Without RF switching, $L = N_\text{b}$, and $\mathbf{T}$ is a DFT unitary matrix such that $\mathbf{T}^\text{H}\mathbf{T} = \mathbf{I}_{N_\text{b}}$. In this case, the Rotman lens is equivalent to a ULA, and hence we also anticipate their interference behavior to be the same. Without RF switching, the expected interference power averaged over payload data and the terminal locations is given by

$$I_1^{\text{RLnoSel}} = \rho_\text{x}(N_\text{u}-1)\,\mathbb{E}\left\{\left|\mathbf{h}_1^\text{H}\,\mathbf{h}_j\right|^2\right\}, \quad (20)$$

where both $\mathbf{h}_1$ and $\mathbf{h}_j$ follow the classical ULA far–field steering vectors. The literature contains many investigations that study the expected interference behavior of a massive MIMO system operating with a ULA under LoS (see e.g.,

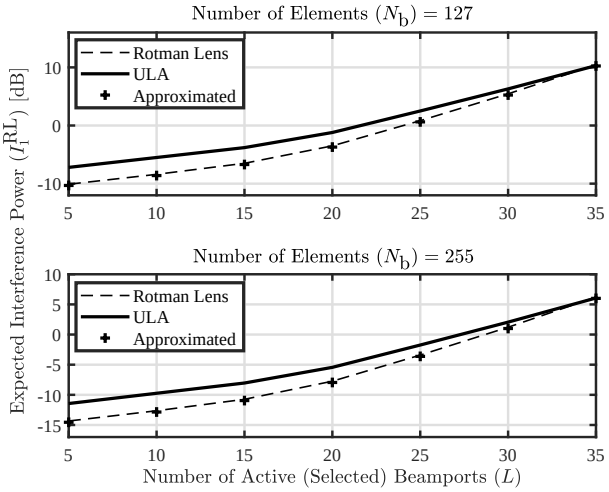

Fig. 4. Expected interference power (I_1^{RL}) vs. the number of active (selected) beamports (L) for different receive array sizes.

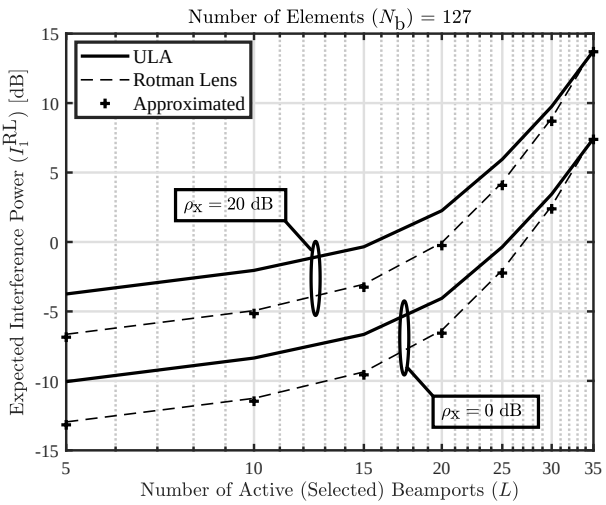

Fig. 5. Expected interference power (I_1^{RL}) vs. the number of selected ports (L) for different uplink SNRs (ρ_{x}).

[24, 25] and references therein). For instance, [25] presents an expression for $\mathbb{E}\left\{|\mathbf{h}_1^{\text{H}}\mathbf{h}_j|^2\right\} = \mu_{1,j}^{\text{RLnoSel}}$, where

$$\mu_{1,j}^{\text{RLnoSel}} = 2\sum_{i=1}^{N_{\text{b}}}\left(1-\frac{i}{N_{\text{b}}}\right)J_0^2\left(\frac{2\pi}{\lambda}\Delta_{\text{i}}\,i\right)+1, \tag{21}$$

giving

$$I_1^{\text{RLnoSel}} = \rho_{\text{x}}\left(N_{\text{u}}-1\right)\mu_{1,j}^{\text{RLnoSel}}. \tag{22}$$

The expected interference performance of both the ULA and the Rotman lens array with and without RF switching is demonstrated in the following section, where the tightness of the derived expressions is numerically evaluated.

V. Numerical Results

The parameters described below are based on a mmWave channel measurement campaign presented in [3]. We consider uplink MU–MIMO operation at a carrier frequency of 28 GHz. A circular coverage radius of $R = 70$ meters is chosen in which the LoS geometric attenuation exponent is $\gamma = 2$. Each terminal is assumed to operate with the same average uplink transmit power, while the noise power at the BS array is assumed to be unity. This implies that ρ_{x}, the average uplink transmit power across the terminals is the also the average uplink signal–to–noise–ratio (SNR). Since the terminals are uniformly distributed with respect to the circular coverage area, the spatial distribution of terminal DoAs $\theta_i \sim \mathcal{U}\left[0, 2\pi\right]$, $\forall i = 1, \ldots, N_{\text{u}}$. The BS array is assumed to be located the origin of the circular area. For both the Rotman lens array and the ULA, the inter–element spacing is $\Delta_{\text{i}} = 0.5\lambda$. Unless otherwise specified, we consider 10^5 channel realizations, $\rho_{\text{x}} = 10$ dB, and a total of $N_{\text{u}} = 40$ terminals in the system.

A. Performance With RF Switching

Figure 4 shows the expected multiuser interference power as a function of L, the number of active (selected) beam ports, considering the Rotman topology, alongside the ULA. The number of receive antennas at the arrays are varied from $N_{\text{b}} = 127$ to $N_{\text{b}} = 255$ to observe the relative change in the interference powers with a fixed ρ_{x} and N_{u}. Considering the performance with $N_{\text{b}} = 127$ antennas, three trends can be seen: (1) As L increases, the average interference power also increases, due to the higher probability of closely spaced terminal DoAs, and smaller angular ranges of each selection bin. (2) While the Rotman lens has a lower average interference power in comparison to the ULA for small L values, for larger L values ($L \geq 30$), the Rotman interference levels approaches to that of the ULA. This is a result of $\mathbf{F}_{\text{RM}}$ matrix becoming increasingly unitary, such that $\mathbf{F}_{\text{RM}}^{\text{H}}\mathbf{F}_{\text{RM}}$ approaches the identity matrix, collapsing the Rotman structure down to a ULA. (3) For each case, the approximated responses demonstrate a tight agreement with the simulated counterparts. Having said the above, it is noteworthy that increasing L may also increase the desired signal power. Hence, increasing L should not be thought of as a catastrophe. The above trends are also visible for the case of $N_{\text{b}} = 255$, although lower interference levels are observed due to the extra degrees of freedom induced by increasing N_{b}.

In similar fashion, Fig. 5 demonstrates the variation of the expected interference power as a function of L for $\rho_{\text{x}} = 0$ and 20 dB, respectively. Naturally, higher interference levels are observed with $\rho_{\text{x}} = 20$ dB in comparison to $\rho_{\text{x}} = 0$ dB, as a higher uplink SNR proportionally scales the interference powers. All other trends are seen to remain unchanged in comparison to Fig. 4.

B. Performance Without RF Switching

We now consider the expected interference performance of the Rotman lens arrays without the presence of RF switching. Specifically, Fig. 6 demonstrates the expected multiuser interference power as a function of an increasing number of terminals. Two critical observations can be made: (1) The interference power is approximately 5 dB higher with the absence of RF switching in comparison to the case with RF switching in Fig. 4. This is due to the absence of any constraints on the separation of terminal DoAs. (2) The interference characteristics of the Rotman lens collapse to that of the ULA, and a clear equivalence between the two cases can be seen across all terminals for both array sizes.

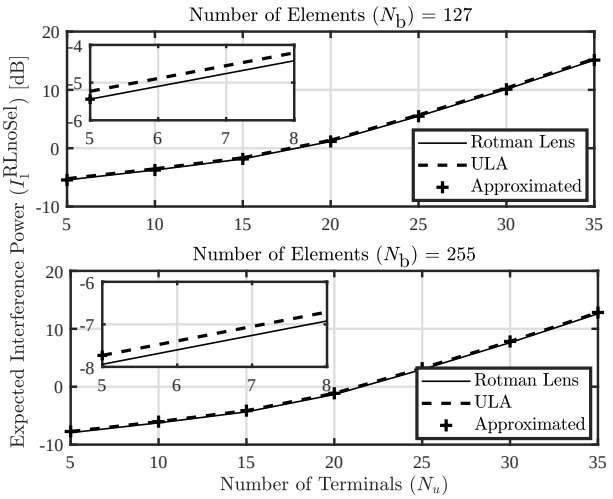

Fig. 6. Expected interference power without RF switching (I_1^{RLnoSel}) vs. the number of user terminals (N_{u}) for different receive array sizes.

A mathematical justification for this phenomenon is given in Remark 1 of the paper. For the Rotman lens array, this observation demonstrates the necessity of having an RF switching network for obtaining better interference characteristics than a conventional ULA in mmWave systems. To this end, we conclude that in LoS scenarios, without RF switching, a Rotman lens array gives no additional benefit in comparison to a conventional ULA. Our derived expressions remain tight for the case when there is no RF switching.

VI. Conclusions

This paper provides insights into the interference behavior of lens–based mmWave MU–MIMO systems, with and without RF switching. Considering LoS propagation, tight analytical expressions for the expected interference power of an arbitrary terminal are derived with Rotman lens antenna arrays. Our expressions show that without RF switching, the Rotman lens losses its benefits and collapses to a conventional ULA. Furthermore, our findings show that the expected interference power significantly decreases with RF switching, as the uplink DoAs can be separated in contrast to no switching, which allows for very similar DoAs. As a whole, our results showcase the necessity of operating Rotman lens antenna arrays with RF switching. As such, the results provide a cautionary tale to potential researchers on the performance similarities and differences between Rotman arrays and ULAs.

VII. Acknowledgment

The work of H. Tataria, M. Matthaiou, and V. F. Fusco was supported by the EPSRC, UK, under grants EP/P000673/1 and EP/EN02039/1. The work of P. J. Smith was supported by the Royal Academy of Engineering, UK, via the Distinguished Visiting Fellowship scheme DVF1617/6/29. The authors thank Prof. Andreas F. Molisch for the insightful discussions during the course of this work.

References

[1] M. Shafi, *et al.*, "5G: A tutorial overview of standards, trials, challenges, deployment, and practice," *IEEE J. Sel. Areas Commun.*, vol. 35, no. 6, pp. 1201-1221, Jun. 2017.

[2] J. Ko, *et al.*, "Millimeter-wave channel measurements and analysis for statistical spatial channel model in in-building and urban environments at 28 GHz," *IEEE Trans. Wireless Commun.*, vol. 16, no. 9, pp. 5853-5868, Sep. 2017.

[3] M. R. Akdeniz, *et al.*, "Millimeter-wave channel modeling and cellular capacity evaluation," *IEEE J. Sel. Areas Commun.*, vol. 32, no. 6, pp. 1164-1179, Jun. 2014.

[4] H. Tataria, P. J. Smith, L. J. Greenstein, P. A. Dmochowski, and M. Matthaiou, "Impact of line-of-sight and unequal spatial correlation on uplink MU-MIMO systems," *IEEE Wireless Commun. Lett.*, vol. 6, no. 5, pp. 634-637, Oct. 2017.

[5] A. F. Molisch, *et al.*, "Hybrid beamforming for massive MIMO: A survey," *IEEE Commun. Mag.*, vol. 55, no. 9, pp. 134-141, Sep. 2017.

[6] W. Hong *et al.*, "Multibeam antenna technologies for 5G wireless communications," *IEEE Trans. Antennas Propag.*, vol. 65, no. 12, pp. 6231-6249, Dec. 2017.

[7] O. El Ayach, S. Rajagopal, S. Abu-Surra, Z. Pi, and R. W. Heath Jr., "Spatially sparse precoding in millimeter wave MIMO systems," *IEEE Trans. Wireless Commun.*, vol. 13, no. 3, pp. 1499-1513, Mar. 2014.

[8] A. Alkhateeb, G. Leus, and R. W. Heath Jr., "Limited feedback hybrid precoding for multi-user millimeter wave systems," *IEEE Trans. Wireless Commun.*, vol. 14, no. 11, pp. 6481-6494, Nov. 2015.

[9] X. Gao, *et al.*, "Energy-efficient hybrid analog and digital precoding for mmWave MIMO systems with large antenna arrays," *IEEE J. Sel. Areas Commun.*, vol. 34, no. 4, pp. 998-1009, Apr. 2016.

[10] V. Raghavan, *et al.*, "Single-user vs. multi-user precoding for millimeter-wave MIMO systems," *IEEE J. Sel. Areas Commun.*, vol. 35, no. 6, pp. 1387-1401, Jun. 2017.

[11] S. Park, A. Alkhateeb, and R. W. Heath Jr., "Dynamic subarrays for hybrid precoding in wideband mmWave MIMO systems," *IEEE Trans. Wireless Commun.*, vol. 16, no. 5, pp. 2907-2920, May 2017.

[12] J. Brady, N. Behdad, and A. M. Sayeed, "Beamspace MIMO for millimeter-wave communications: System architecture, modeling, analysis, and measurements," *IEEE Trans. Antennas Propag.*, vol. 6, no. 7, pp. 3814-3827, Jul. 2013.

[13] A. M. Sayeed and N. Behdad, "Continuous aperture phased MIMO: Basic theory and applications," in *Proc. IEEE 48th Annu. Allerton Conf. Commun., Control, and Computing*, Sep. 2010, pp. 1196-1203.

[14] Y. Gao, M. Khaliel, F. Zheng, and T. Kaiser, "Rotman lens based hybrid analog-digital beamforming in massive MIMO systems: Array architectures, beam selection algorithms and experiments", *IEEE Trans. Veh. Technol.*, Jun. 2017.

[15] Y. Zeng and R. Zhang, "Millimeter wave MIMO with lens antenna array: A new path division multiplexing paradigm," *IEEE Trans. Commun.*, vol. 64, no. 4, pp. 1557-1571, Apr. 2016.

[16] Y. Zeng , L. Yang, and R. Zhang, "Multi-user millimeter wave MIMO with single-sided full-dimensional lens antenna array," in *Proc. IEEE ICC*, May 2017.

[17] A. M. Sayeed and J. Brady, "Beamspace MIMO channel modeling and measurement: Methodology and results at 28GHz," in *Proc. IEEE GLOBECOM (Workshops)*, Dec. 2016.

[18] T. Kwon, Y-G. Lim, B-W. Min, and C-B. Chae, "RF lens-embedded massive MIMO systems: Fabrication issues and codebook design," *IEEE Trans. Microw. Theory Techn.*, vol. 64, no. 7, pp. 2256-2271, Jul. 2016.

[19] A. M. Sayeed, "Deconstructing multiantenna fading channels," *IEEE Trans. Signal Process.*, vol. 50, no. 10, pp. 2563-2579, Oct. 2002.

[20] J. Brady and A. M. Sayeed, "Beamspace MU-MIMO for high-density gigabit small cell access at millimeter wave frequencies," in *Proc. IEEE SPAWC*, Jun. 2014, pp. 80-84.

[21] X. Gao, L. Dai, S. Han, C-Lin I, X. Wang, "Reliable Beamspace Channel estimation for millimeter-wave massive MIMO systems with lens antenna array," *IEEE Trans. Wireless Commun.*, vol. 16, no. 9, pp. 6010 - 6021, Sep. 2017.

[22] A. Adhikary, A. Ashikhmin, and T. L. Marzetta, "Uplink interference reduction in large-scale antenna systems," *IEEE Trans. Commun.*, vol. 65, no. 5, pp. 2194-2206, May 2017.

[23] K. V. Mardia, P. J. Zemroch, "The von Mises distribution function," *J. Royal Statistical Soc.*, vol. 24, no. 2, pp. 268-272, Feb. 1975.

[24] H. Yang and T. L. Marzetta, "Massive MIMO with max-min power control in line-of-sight propagation environment," *IEEE Trans. Commun.*, Jul. 2017.

[25] W. Tan, P. J. Smith, H. A. Suraweera, M. Matthaiou, and S. Jin, "Spectral efficiency of multi-user mmWave systems with uniform linear arrays and MRT," in *Proc. IEEE VTC-Spring*, May 2016.